Front. Med. 2025, 19(3): 507−522
https://doi.org/10.1007/s11684-025-1132-8

RESEARCH ARTICLE

Determining the biomarkers and pathogenesis of myocardial infarction combined with ankylosing spondylitis via a systems biology approach

Chunying Liu[1,2,*], Chengfei Peng[2,*], Xiaodong Jia[2], Chenghui Yan[2], Dan Liu[2], Xiaolin Zhang[2], Haixu Song (✉)[2], Yaling Han (✉)[1,2]

[1]*Beifang Hospital of China Medical University, Shenyang 110016, China;* [2]*State Key Laboratory of Frigid Zone Cardiovascular Diseases (SKLFZCD), Cardiovascular Research Institute and Department of Cardiology, Shenyang 110016, China*

Abstract **Ankylosing spondylitis (AS) is linked to an increased prevalence of myocardial infarction (MI). However, research dedicated to elucidating the pathogenesis of AS-MI is lacking. In this study, we explored the biomarkers for enhancing the diagnostic and therapeutic efficiency of AS-MI. Datasets were obtained from the Gene Expression Omnibus database. We employed weighted gene co-expression network analysis and machine learning models to screen hub genes. A receiver operating characteristic curve and a nomogram were designed to assess diagnostic accuracy. Gene set enrichment analysis was conducted to reveal the potential function of hub genes. Immune infiltration analysis indicated the correlation between hub genes and the immune landscape. Subsequently, we performed single-cell analysis to identify the expression and subcellular localization of hub genes. We further constructed a transcription factor (TF)-microRNA (miRNA) regulatory network. Finally, drug prediction and molecular docking were performed. *S100A12* and *MCEMP1* were identified as hub genes, which were correlated with immune-related biological processes. They exhibited high diagnostic value and were predominantly expressed in myeloid cells. Furthermore, 24 TFs and 9 miRNA were associated with these hub genes. Enzastaurin, meglitinide, and nifedipine were predicted as potential therapeutic agents. Our study indicates that *S100A12* and *MCEMP1* exhibit significant potential as biomarkers and therapeutic targets for AS-MI, offering novel insights into the underlying etiology of this condition.**

Keywords myocardial infarction; ankylosing spondylitis; inflammation; bioinformatics analysis

Introduction

The occurrence of myocardial infarction (MI), which is characterized by the accumulation of atherosclerotic plaques, inflammation, and endothelial dysfunction, represents a prominent cause of morbidity and mortality on a global scale [1,2]. Cardiomyocyte death, which plays a pivotal role in myocardial injury followed by MI, is frequently attributed to an intense inflammatory response [3]. Previous studies have demonstrated that the complex inflammatory response aroused in MI is highly associated with the activation of a cascade of inflammatory signaling pathways [4].

Ankylosing spondylitis (AS) is an inflammatory rheumatic disease characterized by progressive and debilitating arthritis that involves the axial bones [5]. Typical clinical features of AS include inflammatory back pain, decreased spinal mobility, oligoarthritis, enthesitis, and dactylitis [6]. The latest research findings indicate that AS typically manifests before the age of 45 years and exhibits a high incidence rate, leading to diminished quality of life and detrimental psychological and physiologic effects [7]. The prevailing belief is that AS serves as a precipitating factor for MI and exacerbates the severity of cardiac injury, augmenting mortality risk in patients with AS-MI [8]. The higher cardiovascular mortality and morbidity rates observed in AS may be attributed to the systemic inflammation [9]. However, research on the pathogenesis of AS-MI remains scarce.

Received October 28, 2024; accepted January 9, 2025
Correspondence: Yaling Han, hanyaling@163.net;
Haixu Song, haixu0215@163.com

*The authors contributed equally to this work.

Here, we identified biomarkers involved in the pathogenesis of AS-MI and provided novel targets for clinical diagnosis and treatment. This study screened available AS and MI datasets to look for co-expressed differentially expressed genes (C-DEGs) and the hub genes were further identified via machine learning models. Gene set enrichment analysis (GSEA) was performed to explore the underlying functions of hub genes. Subsequently, a receiver operating characteristic (ROC) curve and a nomogram were designed to demonstrate accuracy for clinical prediction. In addition, we found the link between hub genes and the immune landscape, while single-cell analysis identified the expression and cell location of hub genes. Finally, drug prediction was performed through CMap and AutoDock Tools. The present study is the first to determine the underlying pathogenesis of AS-MI and provide predictive biomarkers for its diagnosis and treatment. The analytical workflow is illustrated in detail in Fig. 1.

Materials and methods

Collection and processing of microarray data

The MI data sets (GSE66360 and GSE60993) and AS data sets (GSE25101 and GSE73754) were obtained from the Gene Expression Omnibus (GEO) database. Among them, GSE66360 and GSE25101 were selected for differentially expressed gene (DEG) screening, while GSE60993 and GSE73754 were utilized for model testing. The characteristics of the data sets are provided in Table S1.

DEG analysis

The DEGs in the GSE66360 and GSE25101 data set were analyzed using the "limma" package with the standard of $|\log_2 FC| > 0.585$ and P value < 0.05. The ClueGO plug-in in Cytoscape software was used to construct a PPI network for the top 50 DEGs in the MI and AS data sets,

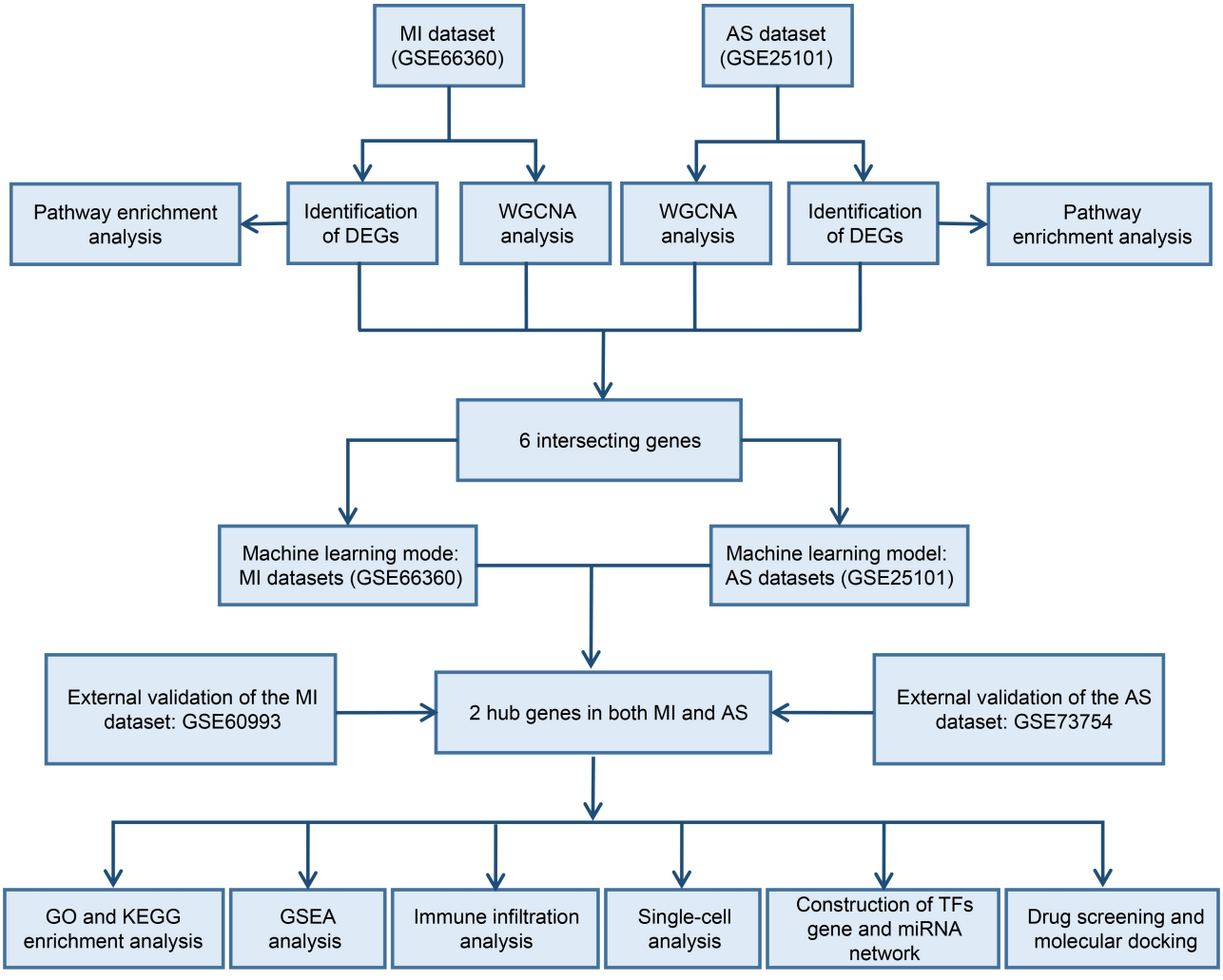

Fig. 1 Inclusion of literature flowchart.

and the functions of these important DEGs were further analyzed.

Weighted gene co-expression network analysis (WGCNA)

To identify the potential hub genes associated with disease phenotypes, we employed the WGCNA algorithm to construct a gene co-expression network. Adjacency was calculated by setting the soft threshold of the MI data set to seven and the soft threshold of the AS data set to five. The correlation coefficients between the modules and clinical features of MI and AS were separately calculated, followed by the selection of genes in the modules with $|Cor| > 0.4$ for further analysis.

Building of machine learning models and validation of hub genes

Machine learning models were employed using the "caret" package, which included the support vector machine (SVM), random forest (RF), generalized linear model (GLM), *k*-nearest neighbor (*k*-NN), and least absolute shrinkage and selection operator (LASSO). All five machine learning models were executed with default parameters and evaluated through fivefold cross-validation. The ROC curve and nomogram were used to evaluate the accuracy of S100A12 and MCEMP1 in relevant model prediction, aiming to identify potential biomarkers related to AS-MI.

Verification of hub genes and construction of PPI network

The "ggplot2" package was utilized to generate a boxplot (Wilcoxon test) for visualizing the expression of hub genes in the MI-GSE66360 and AS-GSE25101 data sets and subsequently validate the hub genes that use the testing data sets GSE60993 and GSE73754. The GeneMANIA website was used to construct the PPI network for hub genes, while the "ClusterProfiler" package was utilized to perform Gene Ontology (GO) and Kyoto Encyclopedia of Genes and Genomes (KEGG) analysis on the functional features of genes in the PPI network.

GSEA

The samples were classified into two groups, namely, the high and low expression groups, based on the median of hub genes. Differential gene analysis was performed using the "limma" algorithm, followed by GSEA using the "ClusterProfiler" package to assess and visualize the significant pathways ($P < 0.05$) in the group with a high expression of hub genes.

Immune infiltration analysis

To investigate the correlation between hub genes and immune cell infiltration, we used the ESTIMATE algorithm to analyze the infiltration levels of immune cells. The correlation between hub genes and Estimate score was presented through scatterplots. The violin plot was drawn using the "ggplot2" package to check whether immune cell content was different between the disease sample and the normal sample ($P < 0.05$). The correlation of the 2 hub genes with 28 types of immune cells was examined using the single-sample GSEA (ssGSEA) algorithm. Then, we used heat maps to show the correlations between hub genes and immune cell markers. GO and KEGG pathway sets were comprehensively scored using the gene set variation analysis (GSVA) algorithm, and the correlation between immune pathways and hub genes in MI and AS was analyzed.

Single-cell analysis

The single nucleus RNA sequencing data set (GSE214611) was obtained from the GEO database, and the Seurat V4.1.0 software package was used for subsequent analysis [10]. After performing quality control and filtration, we conducted cluster analysis and utilized the t-distributed stochastic neighbor embedding format to visualize these clusters. The cell type was subsequently determined using the findallmarkers () function of the "Seurat" package, enabling identification of the composition of distinct cell subpopulations across different samples.

Construction of the transcription factor (TF)-microRNA (miRNA) regulatory network

We utilized the miRNet2.0 online database to screen for miRNA and TFs associated with hub genes and subsequently identified and constructed a network by using Cytoscape software.

Drug screening and molecular docking

Target drugs for hub genes were predicted using the CMap database. Subsequently, AutoDockVina software [11] was used to dock the predicted drug molecules with two hub genes, and Discovery Studio software was used for visualization.

Results

Identification of DEGs

Differential analysis between 50 normal and 49 MI

samples in GSE66360 revealed 1 222 DEGs. Among which, 700 were upregulated and 522 were downregulated. A volcano plot was drawn to depict DEG expression (Fig. 2A), and the top 50 DEGs were selected to create a heat map (Fig. 2B). Simultaneously, we utilized the ClueGO plugin of Cytoscape software to construct a pathway network and investigate the functions of the top 50 DEGs associated with MI. The results revealed that these genes were primarily associated with the "cellular defense response," "neutrophil chemotaxis," and "IL-10 signaling." Furthermore, other signaling pathways, including "neutrophil migration" and "interleukin-2 production," were also identified. The findings suggest that these DEGs play a regulatory role in MI by modulating immune responses and inflammatory signaling pathways (Fig. 2C). Moreover, 62 DEGs were identified in GSE25101, including 48 upregulated genes and 14 downregulated genes. These DEGs were visualized through a volcano plot (Fig. 2D) with downregulated genes in blue and upregulated genes in yellow. We also chose the top 50 DEGs to create a heat map (Fig. 2E) and explored the functions of these DEGs in the GSE25101 data set. The top 50 DEGs were also predominantly enriched in inflammatory signaling pathways, such as "interleukin-1 signaling" and "the regulation of RUNX2 expression and activity" (Fig. 2F).

Identification of modules linked to the clinical features of MI and AS via WGCNA

WGCNA was utilized to construct a co-expression network for the MI and AS data sets and identify co-expression modules. After conducting hierarchical clustering analysis, neither the MI nor the AS data set yielded any statistically significant abnormal samples. We set the optimal soft threshold for the MI data set to 7 (R^2 = 0.85) and that for the AS data set to 5 (R^2 = 0.85) (Fig. 3A and 3B). Subsequently, the DEGs that exhibited similar expression patterns were organized into modules through hierarchical clustering analysis. Thus, 18 modules were identified in the MI data set and 29 modules were identified in the AS data set (Fig. 3C and 3D). The correlation between each module and clinical features was subsequently computed and the modules with |Cor| > 0.4 were selected for further analysis. In the AMI network, the grey60 (Cor = 0.48, P = 1e−06), yellow (Cor = 0.61, P = 8e−11), and purple (Cor = 0.60, P = 2e−10) modules were identified as key modules. In the AS network, the darkred (Cor = −0.41, P = 0.04), grey60 (Cor = −0.49, P = 0.01), yellow (Cor = –0.41, P = 0.04), purple (Cor = 0.56, P = 0.003), cyan (Cor = −0.49, P = 0.01), and lightcyan (Cor = –0.63, P = 7e−04) modules were selected as key modules (Fig. 3E and 3F).

Screening of C-DEGs

To further screen DEGs, we first employed Venn diagrams to identify six DEGs (Fig. 4A). Then, five machine learning models were constructed using the "DALEX" package. We evaluated the predictive performance of the five machine learning models by constructing ROC curves. The *k*-NN model exhibited the largest area under the curve (AUC) = 0.897 in the MI data sets (Fig. 4B) and the top three important DEGs in each model were displayed (Fig. 4C). The *k*-NN model in the AS data set also demonstrated superior predictive ability compared with the four other models (Fig. 4D), and the top three significant DEGs of each model were presented (Fig. 4E). Finally, we intersected the DEGs obtained from the *k*-NN model through Venn diagrams, and thus, *S100A12* and *MCEMP1* were selected as potential biomarkers for subsequent analysis (Fig. 4F). The diagnostic performance of the two hub genes was evaluated with ROC curves, and they presented satisfactory performance. In the MI data set, *S100A12* exhibited high accuracy (AUC = 0.893), followed by *MCEMP1* (AUC = 0.838) (Fig. 4G). Meanwhile, a nomogram that incorporated the two significant risk factors was constructed, highlighting their superior diagnostic value for predicting MI (Fig. 4H). In addition, *S100A12* (AUC = 0.816) and *MCEMP1* (AUC = 0.781) also demonstrated high accuracy in the AS data set (Fig. 4I). The construction of the nomogram revealed that *S100A12* and *MCEMP1* exhibited excellent predictive performance for AS (Fig. 4J). We further validated the hub genes in the testing data sets (GSE60993 and GSE73754), and the result also showed high prediction capacity (Fig. S1A and S1B). Consequently, the data revealed that *S100A12* and *MCEMP1* can be considered potential diagnostic biomarkers for predicting AS-MI patients.

Functional enrichment and pathway analysis of hub genes

We first evaluated the expression of the two hub genes in the MI and AS data sets, and the findings revealed a significant upregulation of *S100A12* and *MCEMP1* expression in the MI group compared with the normal group in the GSE66360 and GSE60993 data sets (Fig. 5A and 5B). This conclusion was significantly consistent with the expression of the two hub genes in the AS data sets (Fig. 5C and 5D). A PPI network was constructed to reveal the interaction of the two hub genes and the potential mechanism, as performed via the GeneMANIA website (Fig. 5E). We then used the "ClusterProfiler" package to conduct GO and KEGG enrichment analysis of genes in the PPI network. The enriched KEGG pathway exhibited a strong correlation with the "IL-17

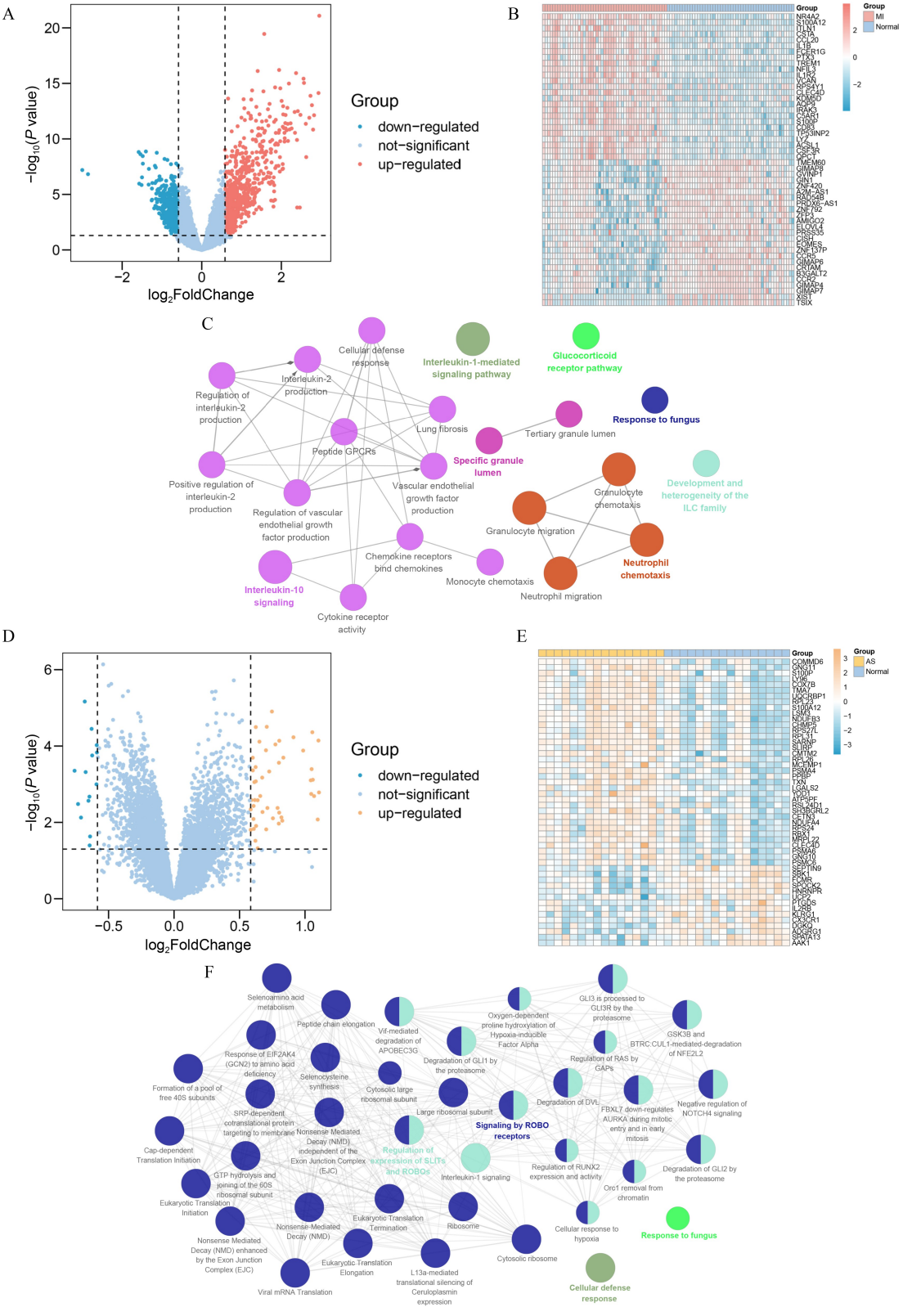

Fig. 2 Identification of DEGs. (A) Volcano plot that shows the DEGs between MI and normal samples in the GSE66360 cohort. (B) The heat map that displays the expression of the top 50 DEGs in the GSE66360 cohort. (C) The pathway enrichment network of the top 50 DEGs in the GSE66360 cohort. (D) Volcano plot that shows the DEGs between AS and normal samples in the GSE25101 cohort. (E) The heat map that displays the expression of the top 50 DEGs in the GSE25101 cohort. (F) The pathway enrichment network of the top 50 DEGs in the GSE25101 cohort.

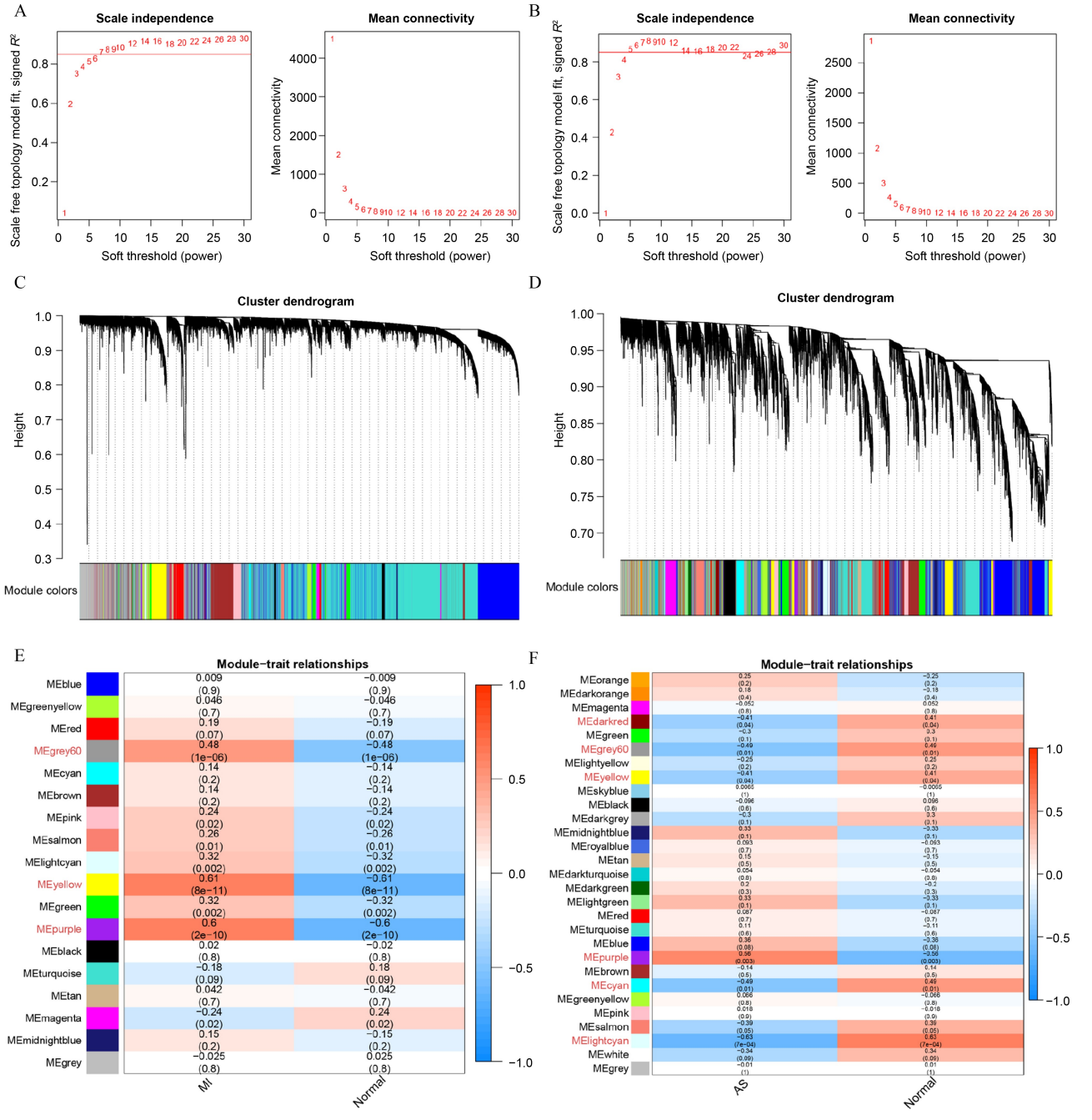

Fig. 3 Identification of modules linked to the clinical features of MI and AS via WGCNA. (A, B) Soft threshold selection process in MI (A) and AS (B). (C, D) Cluster tree dendrogram of co-expression modules in MI (C) and AS (D). (E, F) Heat map of module–trait relationships in MI (E) and AS (F).

signaling pathway" and "neutrophil extracellular trap formation" (Fig. 5F). Alternatively, the GO analysis also revealed enrichment in the "regulation of inflammatory response," "positive regulation of nuclear factor (NF)-κB TF activity" and "RAGE receptor binding" (Fig. 5G). GSEA was performed to identify the signaling pathways associated with *S100A12* and *MCEMP1* in the pathogenesis of AS-MI. The results revealed that the signaling pathway activated by a high expression of *S100A12* was primarily enriched in immune and inflammatory responses, encompassing "neutrophil migration", "positive regulation of the Wnt signaling pathway", and "humoral immune response" (Fig. 5H and 5J). Similarly, the GSEA of *MCEMP1* indicated a positive correlation with inflammation signaling pathways (Fig. 5I and 5K). These findings suggest that

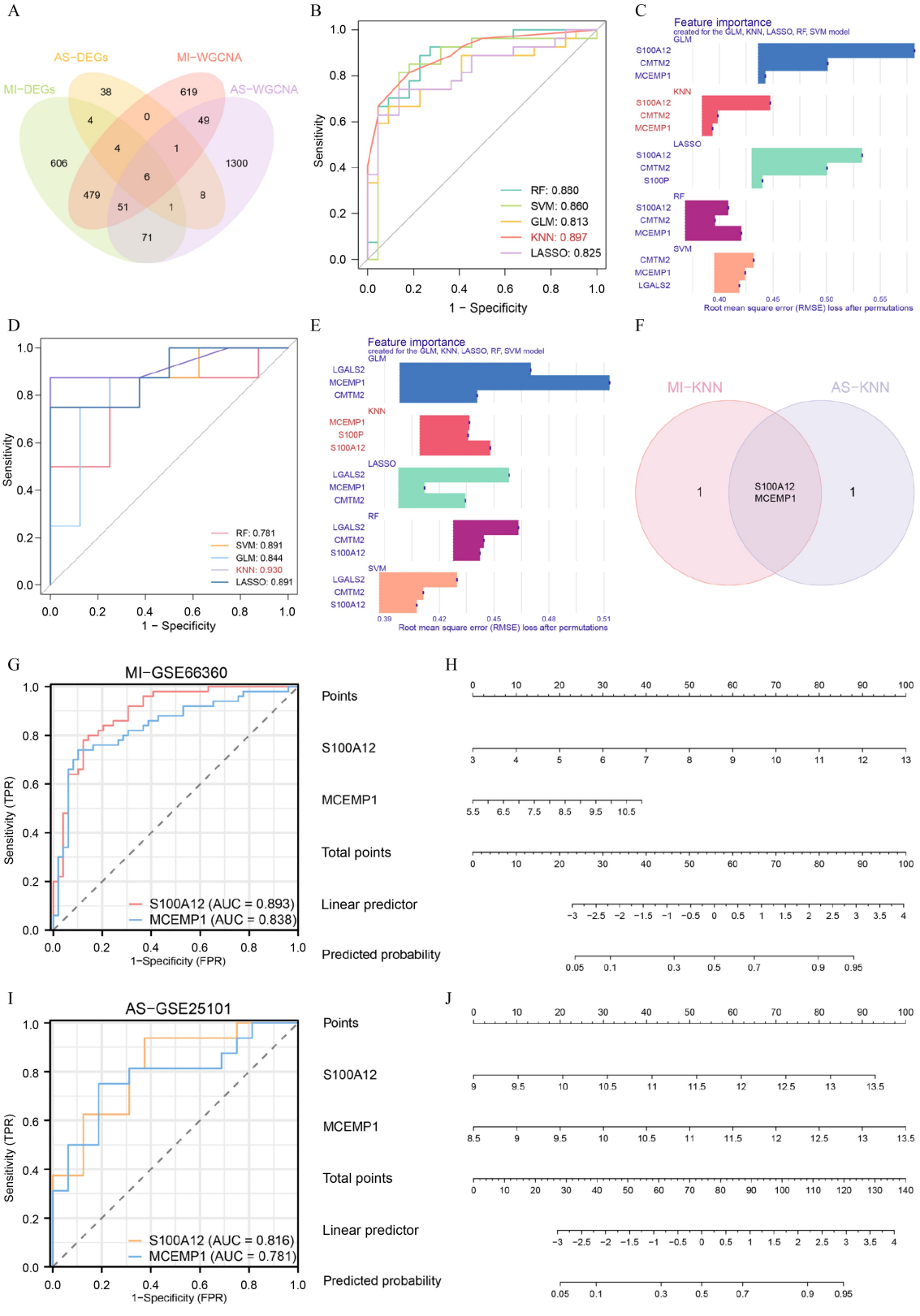

Fig. 4 Screening of C-DEGs. (A) The Venn diagram that shows six important genes that overlap with the DEGs of AS-MI and the key module genes of WGCNA. (B, D) ROC analysis of five machine learning algorithms based on fold cross-validation in the MI (B) and AS (D) cohorts. (C, E) Important features in the RF, SVM, GLM, *k*-NN, and LASSO machine models in the MI (C) and AS (E) cohort. (F) The Venn diagram that shows the intersection of the best model results in the MI and AS cohorts. (G) ROC curves of hub genes in the GSE66360 cohort. (I) ROC curves of hub genes in the GSE25101 cohort. (H, J) Construction of a nomogram for predicting the risk of hub genes in the MI (H) and AS (J) cohorts.

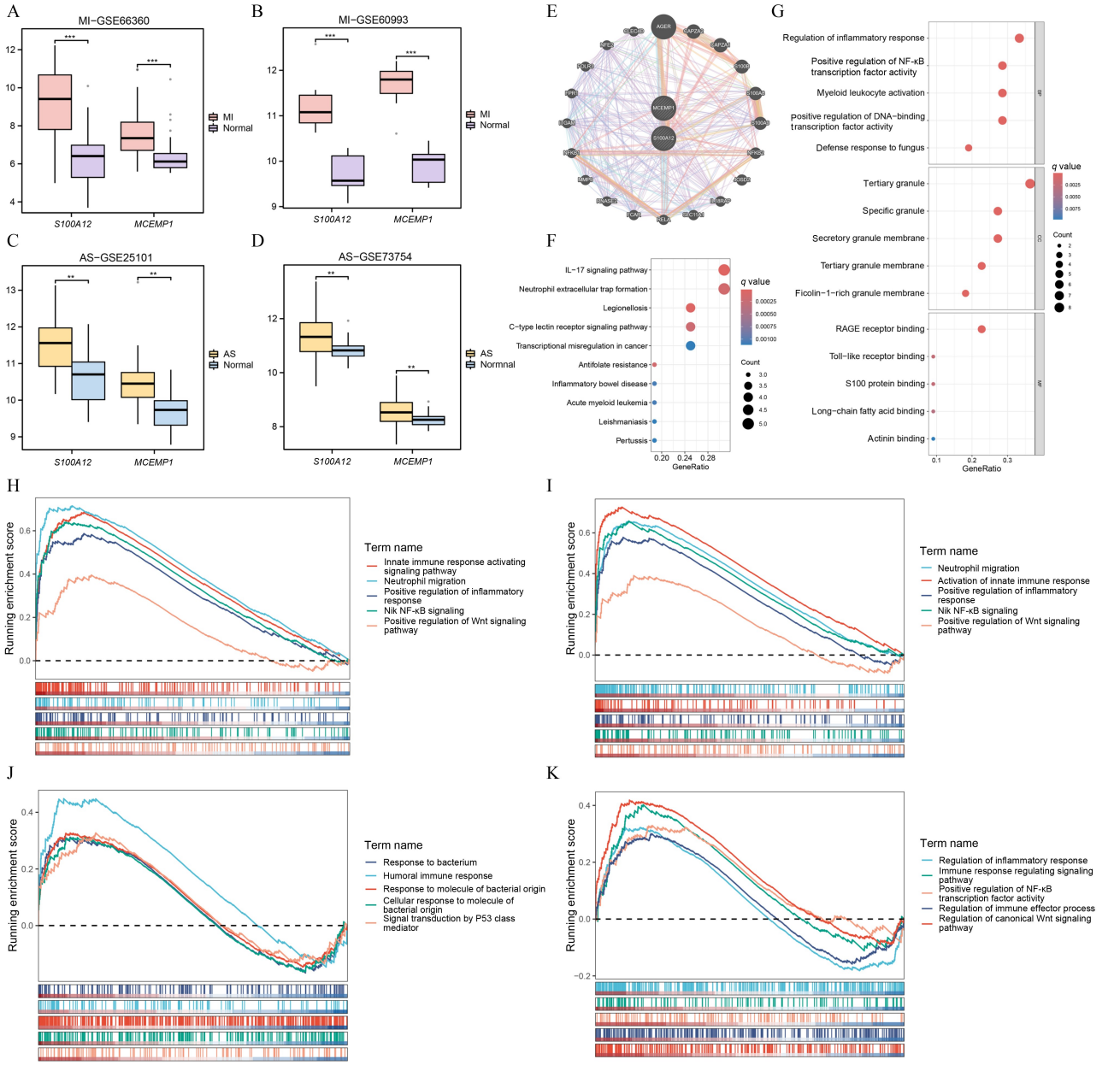

Fig. 5 Functional enrichment and pathway analysis of hub genes. (A, B) Expression of *S100A12* and *MCEMP1* in MI-GSE66360 (A) and MI-GSE60993 (B). (C, D) Expression of *S100A12* and *MCEMP1* in AS-GSE25101 (C) and AS-GSE73754 (D). (E) Construction of the PPI network with the GeneMANIA database. (F) KEGG analysis of genes in the PPI network. (G) GO analysis of genes in the PPI network. (H, I) GSEA of *S100A12* (H) and *MCEMP1* (I) in the MI cohort. (J, K) GSEA of *S100A12* (J) and *MCEMP1* (K) in the AS cohort. $^{**}P < 0.01$; $^{***}P < 0.001$.

the candidate biomarkers are closely associated with inflammatory response in the pathogenesis and development of AS-MI.

Immune infiltration analysis

Given the significant involvement of immune response in the pathogenesis of AS and MI as revealed by functional enrichment analysis, we conducted immune infiltration analysis to evaluate the effect of the two hub genes on immune response. In the MI data set, *S100A12* and *MCEMP1* exhibited a robust correlation with the Estimate score, indicating their extensive involvement in the inflammatory response induced by MI (Fig. 6A and 6B). Similarly, in the AS data set, *S100A12* and *MCEMP1* demonstrated a significant association with the Estimate score (Fig. 6C and 6D). Immune cell content disparity in the MI and AS data sets was assessed using the ssGSEA method. Compared with the normal group, the MI group displayed higher proportions of neutrophils, monocytes, and macrophages, but lower proportions of effector memeory CD8 T cells (Fig. 6E). In addition, the AS

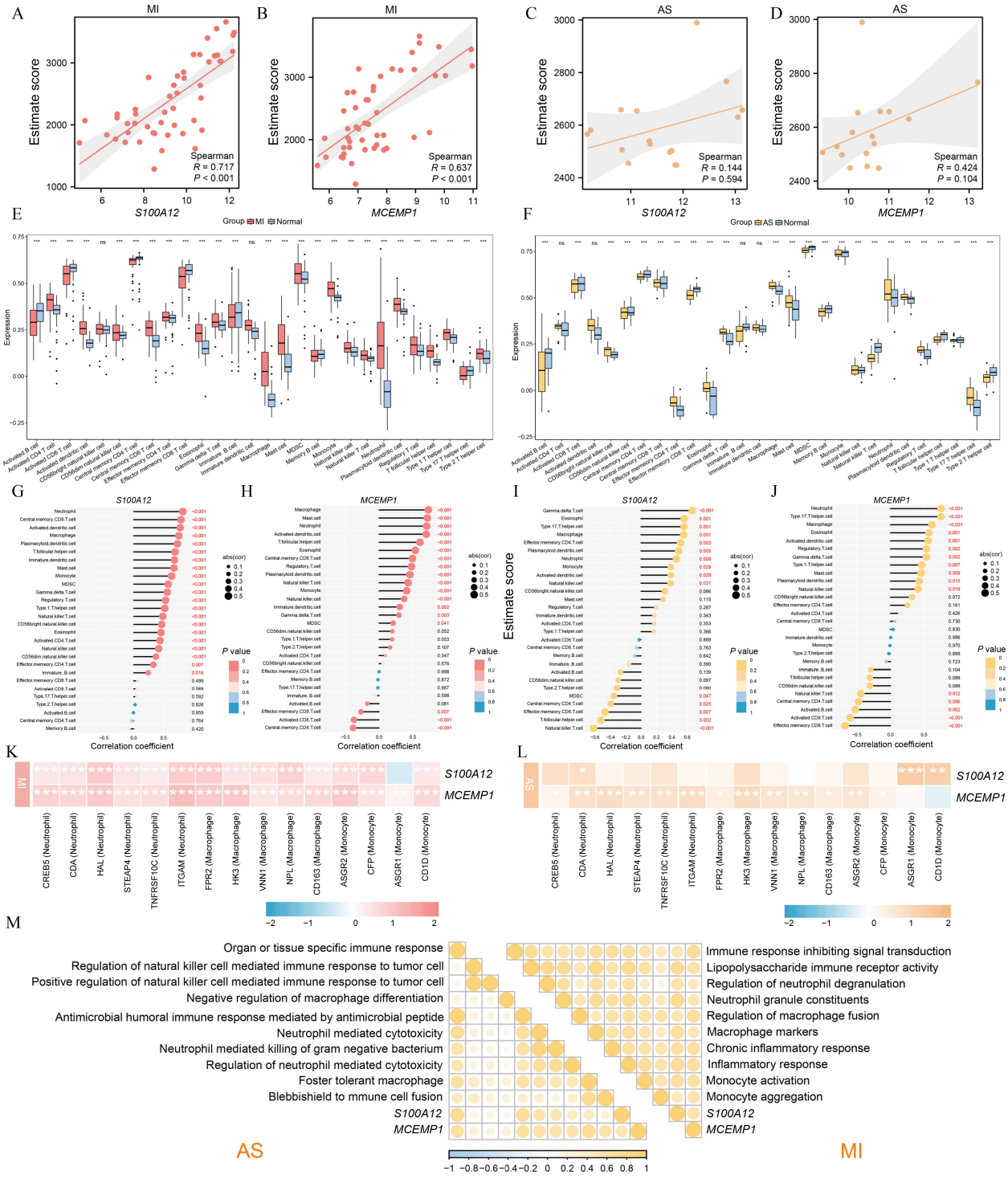

Fig. 6 Immune infiltration analysis. (A, B) Scatterplot of the correlation between the expression levels of the two hub genes and the ESTIMATE score in the MI cohort. (C, D) Scatterplot of correlation between the two hub genes and the ESTIMATE score in the AS cohort. (E) The distribution of 28 immune cells in the MI and normal groups. (F) The distribution of 28 immune cells in the AS and normal groups. (G–J) The lollipop plot that shows the correlation between the expression levels of hub genes and the content of 28 immune cells in MI (G, H) and AS (I, J). (K, L) The heat map that represents Spearman's correlation coefficients between the two hub gene expressions and multiple immune cell marker genes in MI (K) and AS (L). $^{***}P < 0.001$; ns: nonsignificant.

group also exhibited higher proportions of neutrophils, monocytes, and macrophages and lower proportions of effector memeory CD8 T cells compared with the normal group (Fig. 6F). Meanwhile, lollipop plot also showed that *S100A12* and *MCEMP1* were highly correlated with monocytes, macrophages, and neutrophils (Fig. 6G–6J).

Subsequently, we determined the association between hub genes and immune cell biomarkers. The result demonstrated that *S100A12* and *MCEMP1* were significantly correlated with the neutrophil marker cytidine deaminase (CDA) in the AS and MI data sets (Fig. 6K and 6L). In addition, the association of *S100A12* and *MCEMP1* with immune pathways in the MI and AS data sets was further assessed. The findings demonstrated a positive correlation between *S100A12* and *MCEMP1* with various inflammatory signaling pathways, particularly those associated with "organ- or tissue-specific immune response" and "immune response that inhibits signal transduction" **(**Fig. 6M).

Single-cell analysis

We first performed quality control and filtering on 17 samples from the data set GSE214611 to obtain 162 047 cells, which were partitioned into 12 clusters by utilizing principal component analysis with a dimensionality reduction of 20 and a resolution threshold of 0.2 (Fig. S2A and S2B). Based on the cell markers, we further classified the 12 clusters into 4 cell types, namely, cardiomyocytes, fibroblasts, endothelial cells, and myeloid cells (Fig. 7A). GO analysis revealed that marker genes associated with the four cell types were enriched in diverse pathways, indicating substantial heterogeneity among the obtained subtypes based on single-cell RNA sequencing analysis (Fig. 7B). By analyzing the proportion of the four cell types in each sample, the percentage of myeloid cells exhibited a significant increase during the progression of MI, corroborating the aforementioned analysis that highlighted inflammation's pivotal role in the development of MI. The presence of individual outliers within the data can be potentially attributed to sample variations (Fig. 7C). Based on the absence of *S100A12* expression in mice and the structural and functional similarities between *S100A12* and *S100A8/S100A9*, we investigated the expression of *S100A8/S100A9* and *MCEMP1* in the four cell types, revealing their dominant presence in myeloid cells (Fig. 7D). Subsequently, we examined the changes in *S100A8/S100A9* and *MCEMP1* expression during MI and observed a significant surge during the early stages followed by a gradual decrease, confirming their exceptional accuracy and sensitivity for MI diagnosis (Fig. 7E).

Construction of TFs and miRNA regulatory network

To further investigate the regulatory mechanisms of *S100A12* and *MCEMP1*, we conducted a screening of miRNA and TFs associated with hub genes by using the miRNet2.0 online database. In addition, we identified and constructed a network that consisted of 24 TFs and 9 miRNA that are linked to *S100A12* and *MCEMP1* through Cytoscape software (Fig. S3A).

Identification of candidate drugs for AS-MI treatment

Furthermore, we performed candidate drug prediction for *S100A12* and *MCEMP1* to explore potential drugs that might have therapeutic effect on AS-MI patients. We separately uploaded the DEGs obtained from the MI and AS data sets to the CMap database, where we identified a common presence of five drugs (meglitinide, nifedipine, enzastaurin, faropenem, and cytarabine) with the lowest CMap scores in both diseases. The lower the CMap score, the better the treatment effect. The primary mechanism of action for the five drugs involved the inhibition of the protein kinase C (PKC) signaling pathway, and the blockade of potassium and calcium channels, which might have significant therapeutic implications for AS-MI treatment (Table 1).

Molecular docking simulations

The two hub genes exhibited strong affinity with all five drugs, as evidenced by the specific binding energy presented in Table 2. Based on this binding energy, we selected three drugs, namely, enzastaurin, meglitinide, and nifedipine, to perform molecular docking by using AutoDock Tools and AutoDock Vina [11]. The 3D structure of S100A12 and MCEMP1 was obtained from the Uniprot database, and Discovery Studio Visualizer was utilized for visualizing the interaction. Enzastaurin exhibited an alkyl effect with the ALA85, LEU82, LEU4, HIS7, and VAL78 of S100A12, and the docking binding energy was −9.5 kcal/mol (Fig. 8A). Meglitinide forms carbon hydrogen bonds with GLU40 and HIS7 and alkyl bonds with LEU36, VAL78, ILE14, LEU82, LEU77, and PHE74 with binding energy of −8.8 kcal/mol (Fig. 8B). Nifedipine interacts with MET111 of MCEMP1 to form an alkyl bond, and the binding energy was −8.1 kcal/mol (Fig. 8C). In addition, meglitinide interacts with MCEMP1 to form alkyl bonds via VAL125, VAL129, and LYS119 and conventional hydrogen bonds with LEU122, with a docking binding energy of −7.4 kcal/mol (Fig. 8D).

Discussion

The occurrence of MI significantly contributes to the elevated rates of mortality and disability on a global scale, posing a substantial threat to public health worldwide [12,13]. Systemic autoimmune diseases, including rheumatoid arthritis [14], are all related to cardiovascular disease, resulting in a rapid increase in cardiovascular morbidity and mortality [15]. A subtype of autoimmune disease, known as AS, primarily affects the

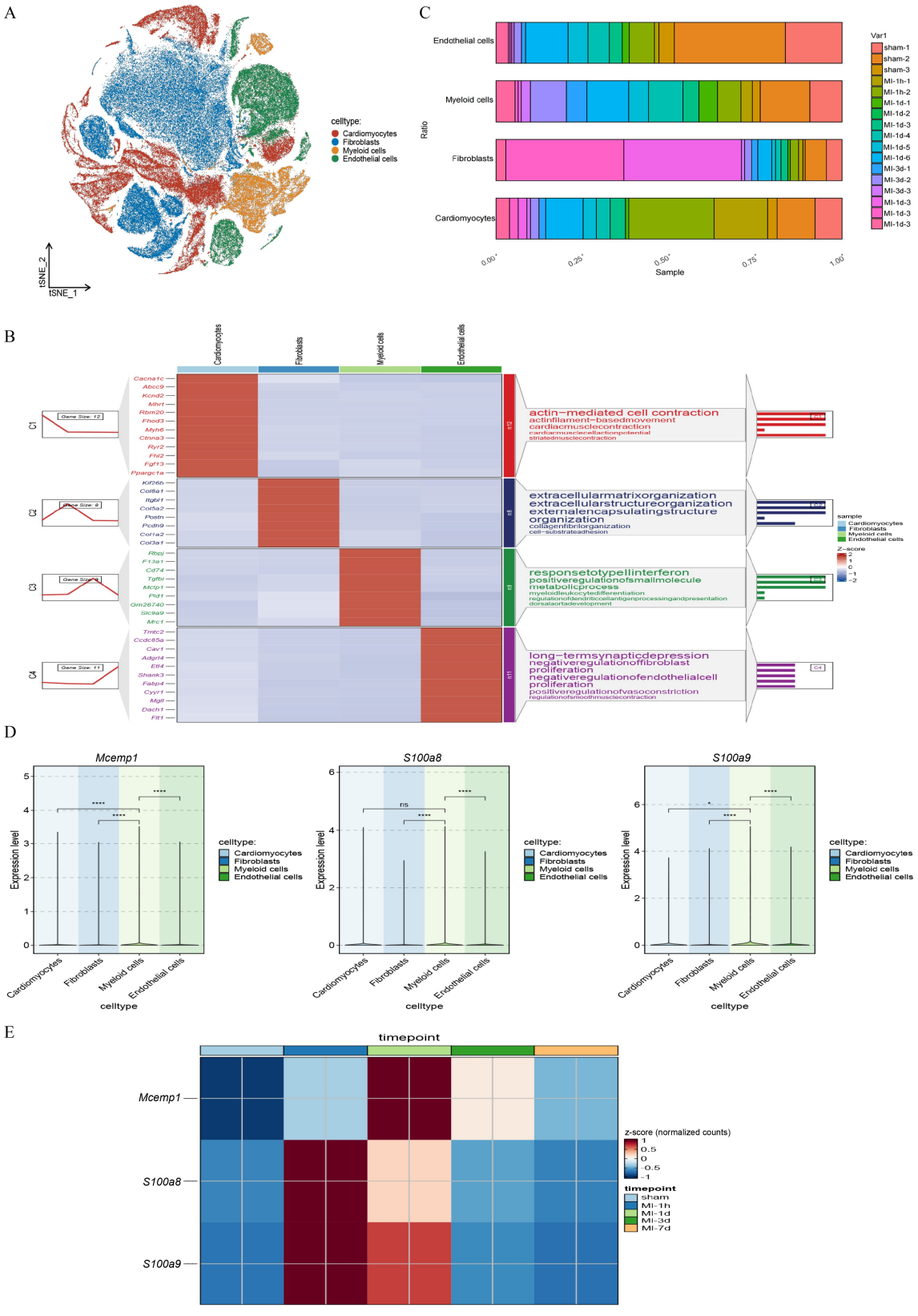

Fig. 7 Single-cell analysis. (A) Cell types were identified by marker genes. (B) The marker genes of the four cell types and the GO analysis of marker genes. (C) The distribution of the four cell types in different samples. (D) The expression levels of *MCEMP1*, *S100A8*, and *S100A9* in the four cell types. (E) The expression levels of *MCEMP1*, *S100A8*, and *S100A9* at different time points of MI. $^{*}P < 0.05$; $^{****}P < 0.001$; ns: nonsignificant.

Table 1 CMap score and molecular action of potential drugs

Drug	CMap score (MI)	CMap score (AS)	Mechanism of action
Meglitinide	−1.6247	−1.54	Potassium channel antagonist
Nifedipine	−1.6315	−1.5394	Calcium channel blocker
Faropenem	−1.5942	−1.5048	Lactamase inhibitor
Enzastaurin	−1.6829	−1.4353	PKC inhibitor
Cytarabine	−1.5387	−1.4197	Ribonucleotide reductase inhibitor

Table 2 Physicochemical and pharmacokinetic properties typical for five small-molecule drugs

Drugs	Binding energy S100A12	Binding energy MCEMP1	LogP	HBD	HBA	PSA	Rotatable bonds
Enzastaurin	−9.5	−7.1	3.7	1	4	72.2 Å	5
Meglitinide	−8.8	−7.4	3.4	2	4	75.6 Å	6
Nifedipine	−8.2	−8.1	2.2	1	7	110 Å	5
Cytarabine	−7.3	−6.9	−2.1	4	5	129 $Å^2$	2
Faropenem	−6.8	−7.0	0.3	2	6	112 Å	3

Note: LogP, lipid–water partition coefficient; HBD, hydrogen bond donor; HBA, hydrogen bond acceptor; MW, molecular weight; PSA, polar surface area.

spinal joints. A growing body of evidence indicates that individuals with AS are predisposed to cardiovascular disease, which is believed to be a consequence of systemic inflammatory response and exhibits greater severity compared with common cardiovascular risk factors [16]. Recently, the largest and longest-lasting national study conducted in the Republic of Korea showed that the risk ratio of MI in the AS group was 1.81 (95% confidence interval was 1.34–2.43). This finding further confirmed that AS is a huge risk factor for MI [17]. In summary, clinical research has established a significant association between MI and AS, indicating that patients with AS are at an elevated risk for developing MI. Therefore, a comprehensive investigation into the mechanism of cardiovascular injury induced by AS and the judicious selection of medications constitute pivotal factors in preventing AS-MI. Given the current absence of AS combined with MI data sets, coupled with a growing body of evidence that highlights the pivotal role of interactions between endothelial cells and peripheral blood cells in the inflammatory milieu of both conditions [18–21], we conducted bioinformatics that used MI (circulating endothelial cells) and AS (peripheral blood cells) data sets to identify important biomarkers of AS-MI and elucidate its underlying molecular mechanisms, providing robust targets for the precise diagnosis and personalized treatment of AS-MI patients.

In the current study, we initially analyzed the DEGs in the MI-GSE66360 and AS-GSE25101 data sets. We observed that the top 50 DEGs were predominantly enriched in the "interleukin-2 production", "neutrophil migration", and other inflammatory signaling pathways. These findings suggest a significant involvement of inflammatory response in the pathogenesis of AS-MI. The activation of pro-inflammatory signaling pathways is known for being critical for the occurrence of MI and the subsequent pathological remodeling [22,23]. Hence, emphasis on inflammatory response has become an essential strategy for cardiac protection and rehabilitation [24,25]. The primary cause of spinal deformity and rigidity is persistent inflammation, while the inhibition of pro-inflammatory factor secretion effectively suppresses ectopic ossification, impeding disease progression [26]. We subsequently conducted WGCNA and machine learning analysis to further identify hub genes. *S100A12* and *MCEMP1* were ultimately selected as hub genes, demonstrating robust predictive capability for the occurrence of AS-MI.

S100A12, located on chromosome 3 in humans, is a member of the S100 calcium binding protein family [27]. S100A12 has been demonstrated to exhibit the ability to bind with and activate cell surface receptors, including Toll-like receptor 4 and G protein-coupled receptors, initiating intracellular inflammatory signal transduction and leading to the induction of pro-inflammatory cytokine expression and involvement in immune and inflammatory regulation [28]. Accelerating reports have identified the important role of S100A12 in rheumatoid arthritis. In a clinical study that involved 42 arthritis patients, the levels of S100A12 in the serum were extremely elevated and then significantly reduced after treatment with metrediene [29]. Moreover, a cohort study that involved 1 023 patients demonstrated that the plasma levels of S100A12 exhibited elevation within a time frame of 30 min and exhibited superior sensitivity compared with cardiac troponin T and creatine kinase-MB (CK-MB) isoenzyme. These findings were further validated in subsequent cohort studies [30]. Hence, we hypothesize that S100A12 may act as a convincing biomarker for the diagnosis and treatment of AS-MI.

MCEMP1 is a protein that spans the entire length of the cell membrane and mostly expressed in mast cells. The

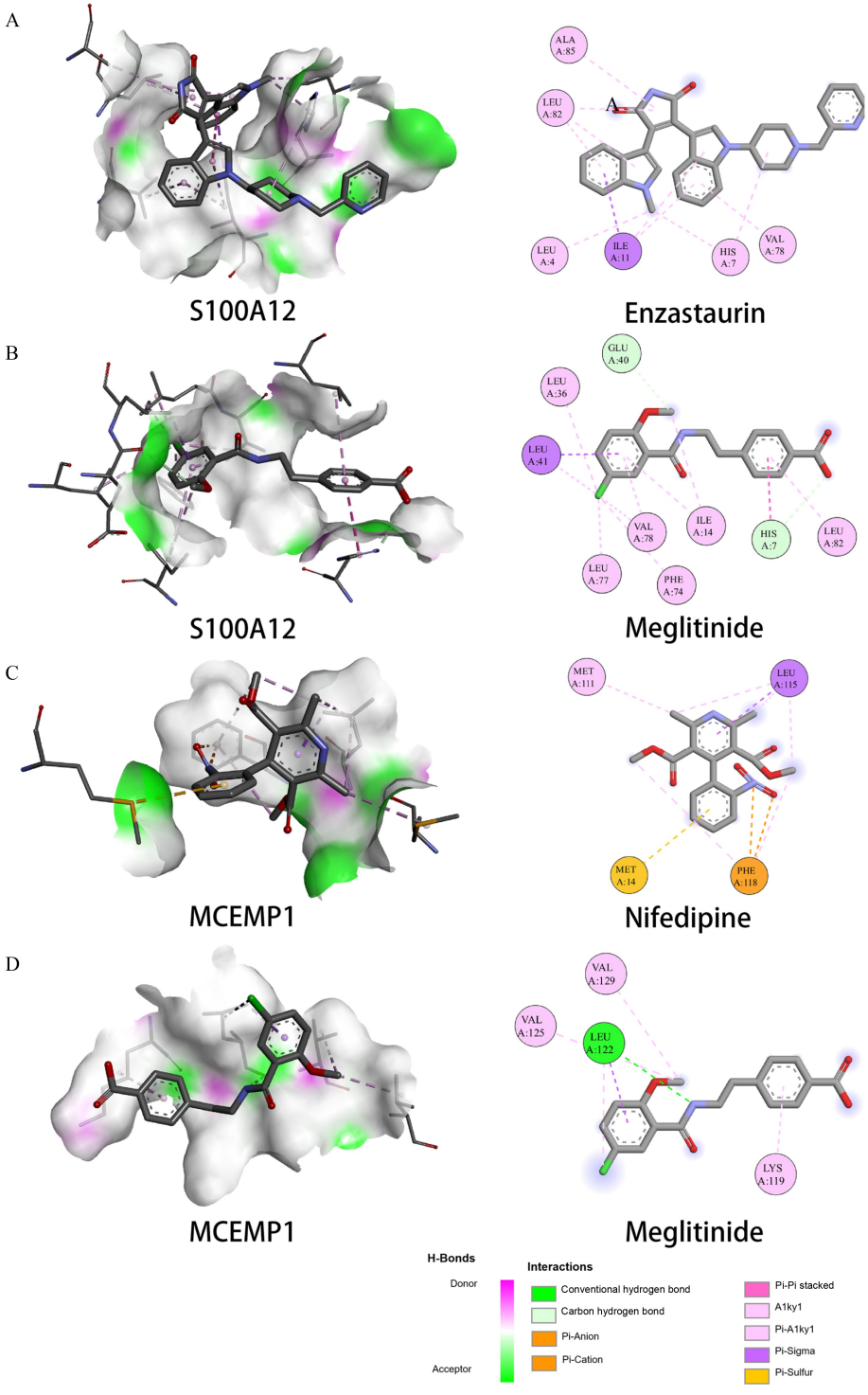

Fig. 8 Molecular docking simulations. (A) Molecular docking pattern between S100A12 and enzastaurin. (B) Molecular docking pattern between S100A12 and meglitinide. (C) Molecular docking pattern between MCEMP1 and nifedipine. (D) Molecular docking pattern between MCEMP1 and meglitinide.

responsibility of MCEMP1 lies in encoding a transmembrane protein with a single channel and participating in the regulation of monocyte differentiation activity or immune responses [31]. MCEMP1 has been identified as a potential prognostic and diagnostic biomarkers for ischemic stroke [32]. Chen *et al*. verified that the inhibition of MCEMP1 could reduce the levels of serum tumor necrosis factor-α, IL-1β and IL-6, weakening the immune activity of sepsis mice [33].

The results of GO and KEGG analysis revealed a

significant involvement of *S100A12* and *MCEMP1* in the pathogenesis of inflammatory and immune responses in AS-MI. Furthermore, the results of GSEA showed that a high expression of *S100A12* and *MCEMP1* was highly correlated with inflammation pathways, such as the NF kappa light chain enhancer of activated B cells (NF-κB) signaling pathway. NF-κB plays a crucial role in regulating inflammatory response, cellular proliferation, and cellular differentiation [34]. Considering the widespread involvement of *S100A12* and *MCEMP1* in inflammatory response and immune processes, we conducted immune infiltration analysis. Compared with normal samples, the MI and AS samples exhibited immune imbalance characterized by a decrease in the levels of immune cells associated with immune defense and an overactivation of immune cells involved in inflammatory response. The results indicated that hub genes were highly correlated with neutrophils, monocytes, and macrophages in the MI and AS data sets. This finding is consistent with the function analysis above. Neutrophils, which comprise the largest proportion of circulating leukocytes in the blood, are quickly recruited to the site of infraction [35]. Emerging evidence has reported that the high correlation between neutrophil extracellular traps and thrombosis is one of the major reasons that leads to the "no-reflow" phenomenon in the pathogenesis of myocardial ischemia-reperfusion injury [36]. In addition, one study reported that neutrophils increased the severity of disease in AS patients by enhancing Th17 response [37]. This finding is highly consistent with the results of our functional enrichment analysis. Monocytes and macrophages play a pivotal role in all three stages of MI, and the excessive infiltration of monocytes and macrophages into the ischemic myocardium has been reported to result in tissue destruction, interstitial fibrosis, and cardiac dysfunction [38]. S100A12, which is mostly secreted by neutrophil granulocytes, exhibits high level in patients who are suffering from various inflammatory disorders [39]. The inhibition of *MCEMP1* by MiRNA-125 results in a reduction in the serum levels of TNF-α, IL-1β, and IL-6, while simultaneously enhancing T lymphocyte viability [40].

We downloaded the single-cell data set to identify cellular heterogeneity and elucidate its underlying mechanisms. Four cell types were identified, namely, cardiomyocytes, fibroblasts, myeloid cells, and endothelial cells. We further analyzed the cellular subsets of these genes and observed their predominant presence in myeloid cells. S100A8, S100A9, and S100A12 belong to the S100 protein family and exhibit a significant level of structural and functional resemblance, which are commonly expressed in neutrophils, macrophages, monocytes, and other immune cells [41]. *S100A12* is absent in mice, but it is located on chromosome 3 between *S100A8* and *S100A9* in humans [42]. Here, we further explored *S100A8* and *S100A9* expression in the scRNA-seq data set. Unexpectedly, a significant increase in *MCEMP1* and *S100A8/S100A9* expression was observed during the early stage of MI. This finding is aligned with previous RNA sequencing findings, providing a direction for further research into the mechanism of comorbidity between AS and MI.

After the identification of hub genes related to AS-MI, we further performed drug prediction with regard to hub genes and provided a new target for AS-MI therapy. Based on the combined score and energy bonding, meglitinide, nifedipine, and enzastaurin were predicted as potential drugs for AS-MI. The meglitinide class of drugs acts as a rapid-acting insulin secretagogue, exerting a significant therapeutic effect on type 2 diabetes mellitus by primarily reducing postprandial blood glucose levels [43]. Nifedipine is a vasodilator calcium antagonist that can increase coronary artery flow in ischemic areas, and it may have a protective effect on ischemic myocardium [44]. Enzastaurin, as a novel antitumor and antiangiogenic drug, exerts its action through the inhibition of PKC, which is a crucial player in the treatment of breast cancer, lung cancer, and other malignancies [45,46].

In the current study, we determined that *S100A12* and *MCEMP1* are upregulated in MI and AS, exhibiting significant diagnostic value. Functional analyses revealed that they are intricately involved in inflammatory responses and immune processes. Furthermore, potential agents that target S100A12 and MCEMP1 were proposed through drug prediction. Consequently, S100A12 and MCEMP1 may serve as promising targets for the diagnosis and treatment of AS-MI. The limitation of this study is the lack of *in vivo* or *in vitro* experimental data to validate and corroborate our findings, although we have endeavored to strengthen the reliability of our conclusions by incorporating MI and AS validation data sets. Consequently, additional experimental research is imperative to validate our results and deepen our comprehension of the underlying mechanisms.

Acknowledgements

This work was supported by the National Natural Science Foundation of China (Nos. 82270300 and 82270493) and the Liaoning Science and Technology Project (Nos. 2024JH2/102500031, 2022JH2/101300012, and 2023-MSLH-344).

Compliance with ethics guidelines

Conflicts of interest Chunying Liu, Chengfei Peng, Xiaodong Jia, Chenghui Yan, Dan Liu, Xiaolin Zhang, Haixu Song, and Yaling Han declare that they have no conflicts of interest.

This is a bioinformatics article and does not involve a research

protocol that requires approval by the relevant institutional review board or ethics committee.

Electronic Supplementary Material Supplementary material is available in the online version of this article at https://doi.org/10.1007/s11684-025-1132-8 and is accessible for authorized users.

References

1. Cai S, Zhao M, Zhou B, Yoshii A, Bugg D, Villet O, Sahu A, Olson GS, Davis J, Tian R. Mitochondrial dysfunction in macrophages promotes inflammation and suppresses repair after myocardial infarction. J Clin Invest 2023; 133(4): e159498
2. Salari N, Morddarvanjoghi F, Abdolmaleki A, Rasoulpoor S, Khaleghi AA, Hezarkhani LA, Shohaimi S, Mohammadi M. The global prevalence of myocardial infarction: a systematic review and meta-analysis. BMC Cardiovasc Disord 2023; 23(1): 206
3. Hu D, Li R, Li Y, Wang M, Wang L, Wang S, Cheng H, Zhang Q, Fu C, Qian Z, Wei Q. Inflammation-targeted nanomedicines alleviate oxidative stress and reprogram macrophages polarization for myocardial infarction treatment. Adv Sci (Weinh) 2024; 11(21): e2308910
4. Pluijmert NJ, de Jong RCM, de Vries MR, Pettersson K, Atsma DE, Jukema JW, Quax PHA. Phosphorylcholine antibodies restrict infarct size and left ventricular remodelling by attenuating the unreperfused post-ischaemic inflammatory response. J Cell Mol Med 2021; 25(16): 7772–7782
5. Ranganathan V, Gracey E, Brown MA, Inman RD, Haroon N. Pathogenesis of ankylosing spondylitis—recent advances and future directions. Nat Rev Rheumatol 2017; 13(6): 359–367
6. van der Linden S, van der Heijde D. Clinical aspects, outcome assessment, and management of ankylosing spondylitis and postenteric reactive arthritis. Curr Opin Rheumatol 2000; 12(4): 263–268
7. Hwang MC, Ridley L, Reveille JD. Ankylosing spondylitis risk factors: a systematic literature review. Clin Rheumatol 2021; 40(8): 3079–3093
8. Peters MJ, Visman I, Nielen MM, Van Dillen N, Verheij RA, van der Horst-Bruinsma IE, Dijkmans BA, Nurmohamed MT. Ankylosing spondylitis: a risk factor for myocardial infarction? Ann Rheum Dis 2010; 69(3): 579–581
9. Mavrogeni S, Servos G, Smerla R, Markousis-Mavrogenis G, Grigoriadou G, Kolovou G, Papadopoulos G. Cardiovascular involvement in pediatric systemic autoimmune diseases: the emerging role of noninvasive cardiovascular imaging. Inflamm Allergy Drug Targets 2015; 13(6): 371–381
10. Butler A, Hoffman P, Smibert P, Papalexi E, Satija R. Integrating single-cell transcriptomic data across different conditions, technologies, and species. Nat Biotechnol 2018; 36(5): 411–420
11. Trott O, Olson AJ. AutoDock Vina: improving the speed and accuracy of docking with a new scoring function, efficient optimization, and multithreading. J Comput Chem 2010; 31(2): 455–461
12. Kim RB, Kim JR, Hwang JY. Epidemiology of myocardial infarction in Korea: hospitalization incidence, prevalence, and mortality. Epidemiol Health 2022; 44: e2022057
13. Su Z, Zou Z, Hay SI, Liu Y, Li S, Chen H, Naghavi M, Zimmerman MS, Martin GR, Wilner LB, Sable CA, Murray CJL, Kassebaum NJ, Patton GC, Zhang H. Global, regional, and national time trends in mortality for congenital heart disease, 1990–2019: an age-period-cohort analysis for the Global Burden of Disease 2019 study. EClinicalMedicine 2022; 43: 101249
14. Xiao ZX, Miller JS, Zheng SG. An updated advance of autoantibodies in autoimmune diseases. Autoimmun Rev 2021; 20(2): 102743
15. Sitia S, Atzeni F, Sarzi-Puttini P, Di Bello V, Tomasoni L, Delfino L, Antonini-Canterin F, Di Salvo G, De Gennaro Colonna V, La Carrubba S, Carerj S, Turiel M. Cardiovascular involvement in systemic autoimmune diseases. Autoimmun Rev 2009; 8(4): 281–286
16. Papagoras C, Voulgari PV, Drosos AA. Cardiovascular disease in spondyloarthritides. Curr Vasc Pharmacol 2020; 18(5): 473–487
17. Park CJ, Choi YJ, Kim JG, Han IB, Do Han K, Choi JM, Sohn S. Association of acute myocardial infarction with ankylosing spondylitis: a nationwide longitudinal cohort study. J Clin Neurosci 2018; 56: 34–37
18. Blanco LP, Wang X, Carlucci PM, Torres-Ruiz JJ, Romo-Tena J, Sun HW, Hafner M, Kaplan MJ. RNA externalized by neutrophil extracellular traps promotes inflammatory pathways in endothelial cells. Arthritis Rheumatol 2021; 73(12): 2282–2292
19. Rengarajan A, Goldblatt HE, Beebe DJ, Virumbrales-Muñoz M, Boeldt DS. Immune cells and inflammatory mediators cause endothelial dysfunction in a vascular microphysiological system. Lab Chip 2024; 24(6): 1808–1820
20. Zhu M, Goetsch SC, Wang Z, Luo R, Hill JA, Schneider J, Morris SM Jr, Liu ZP. FoxO4 promotes early inflammatory response upon myocardial infarction via endothelial Arg1. Circ Res 2015; 117(11): 967–977
21. Ambler WG, Kaplan MJ. Vascular damage in systemic lupus erythematosus. Nat Rev Nephrol 2024; 20(4): 251–265
22. Tong R, Jia T, Shi R, Yan F. Inhibition of microRNA-15 protects H9c2 cells against CVB3-induced myocardial injury by targeting NLRX1 to regulate the NLRP3 inflammasome. Cell Mol Biol Lett 2020; 25(1): 6
23. Prabhu SD, Frangogiannis NG. The biological basis for cardiac repair after myocardial infarction: from inflammation to fibrosis. Circ Res 2016; 119(1): 91–112
24. Broch K, Anstensrud AK, Woxholt S, Sharma K, Tøllefsen IM, Bendz B, Aakhus S, Ueland T, Amundsen BH, Damås JK, Berg ES, Bjørkelund E, Bendz C, Hopp E, Kleveland O, Stensæth KH, Opdahl A, Kløw NE, Seljeflot I, Andersen G, Wiseth R, Aukrust P, Gullestad L. Randomized trial of interleukin-6 receptor inhibition in patients with acute ST-segment elevation myocardial infarction. J Am Coll Cardiol 2021; 77(15): 1845–1855
25. Chen R, Zhao H, Yan H. Long-term management of patients with myocardial infarction: an updated review. Cardiol Discov 2022; 2(4): 241–262
26. Wang L, Wang Y, Jiang Y, Chen M, Li Z, Wang K, Luo C, Ning N, Zeng J, Zhou Z, Song Y, Yang F, Huang SS, Lin Y. Tetrahedral framework nuclear acids can regulate interleukin-17 pathway to alleviate inflammation and inhibit heterotopic ossification in ankylosing spondylitis. ACS Nano 2023; 17(23): 24187–24199
27. Li Y, He Y, Chen S, Wang Q, Yang Y, Shen D, Ma J, Wen Z, Ning S, Chen H. S100A12 as biomarker of disease severity and

prognosis in patients with idiopathic pulmonary fibrosis. Front Immunol 2022; 13: 810338
28. Gonzalez LL, Garrie K, Turner MD. Role of S100 proteins in health and disease. Biochim Biophys Acta Mol Cell Res 2020; 1867(6): 118677
29. Foell D, Kane D, Bresnihan B, Vogl T, Nacken W, Sorg C, Fitzgerald O, Roth J. Expression of the pro-inflammatory protein S100A12 (EN-RAGE) in rheumatoid and psoriatic arthritis. Br J Rheumatol 2003; 42(11): 1383–1389
30. Zhang X, Cheng M, Gao N, Li Y, Yan C, Tian X, Liu D, Qiu M, Wang X, Luan B, Deng J, Wang S, Tian H, Wang G, Ma X, Stone GW, Han Y. Utility of S100A12 as an early biomarker in patients with ST-segment elevation myocardial infarction. Front Cardiovasc Med 2021; 8: 747511
31. Li K, Wang SW, Li Y, Martin RE, Li L, Lu M, Lamhamedi-Cherradi SE, Hu G, Demissie-Sanders S, Zheng J, Chung F, Oates T, Yao Z. Identification and expression of a new type II transmembrane protein in human mast cells. Genomics 2005; 86(1): 68–75
32. Raman K, O'Donnell MJ, Czlonkowska A, Duarte YC, Lopez-Jaramillo P, Peñaherrera E, Sharma M, Shoamanesh A, Skowronska M, Yusuf S, Paré G. Peripheral blood *MCEMP1* gene expression as a biomarker for stroke prognosis. Stroke 2016; 47(3): 652–658
33. Decock J, Hendrickx W, Thirkettle S, Gutiérrez-Fernández A, Robinson SD, Edwards DR. Pleiotropic functions of the tumor- and metastasis-suppressing matrix metalloproteinase-8 in mammary cancer in MMTV-PyMT transgenic mice. Breast Cancer Res 2015; 17(1): 38
34. Oeckinghaus A, Ghosh S. The NF-κB family of transcription factors and its regulation. Cold Spring Harb Perspect Biol 2009; 1(4): a000034
35. Ma Y, Yabluchanskiy A, Lindsey ML. Neutrophil roles in left ventricular remodeling following myocardial infarction. Fibrogenesis Tissue Repair 2013; 6(1): 11
36. Ge L, Zhou X, Ji WJ, Lu RY, Zhang Y, Zhang YD, Ma YQ, Zhao JH, Li YM. Neutrophil extracellular traps in ischemia-reperfusion injury-induced myocardial no-reflow: therapeutic potential of DNase-based reperfusion strategy. Am J Physiol Heart Circ Physiol 2015; 308(5): H500–H509
37. Rosenzweig HL, Vance EE, Asare-Konadu K, Koney KV, Lee EJ, Deodhar AA, Sen R, Caplan L, Napier RJ. Card9/neutrophil signalling axis promotes IL-17A-mediated ankylosing spondylitis. Ann Rheum Dis 2024; 83(2): 214–222
38. Peet C, Ivetic A, Bromage DI, Shah AM. Cardiac monocytes and macrophages after myocardial infarction. Cardiovasc Res 2020; 116(6): 1101–1112
39. Pietzsch J, Hoppmann S. Human S100A12: a novel key player in inflammation? Amino Acids 2009; 36(3): 381–389
40. Chen JX, Xu X, Zhang S. Silence of long noncoding RNA NEAT1 exerts suppressive effects on immunity during sepsis by promoting microRNA-125-dependent MCEMP1 downregulation. IUBMB Life 2019; 71(7): 956–968
41. Xia P, Ji X, Yan L, Lian S, Chen Z, Luo Y. Roles of S100A8, S100A9 and S100A12 in infection, inflammation and immunity. Immunology 2024; 171(3): 365–376
42. Oesterle A, Bowman MA. S100A12 and the S100/Calgranulins: emerging biomarkers for atherosclerosis and possibly therapeutic targets. Arterioscler Thromb Vasc Biol 2015; 35(12): 2496–2507
43. Pakkir Maideen NM, Manavalan G, Balasubramanian K. Drug interactions of meglitinide antidiabetics involving CYP enzymes and OATP1B1 transporter. Ther Adv Endocrinol Metab 2018; 9(8): 259–268
44. Roberts R, Jaffe AS, Henry PD, Sobel BE. Nifedipine and acute myocardial infarction. Herz 1981; 6(2): 90–97
45. Polisety A, Misra G, Rajawat J, Katiyar A, Singh H, Bhatt AN. Therapeutic natural compounds Enzastaurin and Palbociclib inhibit MASTL kinase activity preventing breast cancer cell proliferation. Med Oncol 2022; 39(5): 100
46. Shimokawa T, Seike M, Soeno C, Uesaka H, Miyanaga A, Mizutani H, Kitamura K, Minegishi Y, Noro R, Okano T, Yoshimura A, Gemma A. Enzastaurin has anti-tumour effects in lung cancers with overexpressed JAK pathway molecules. Br J Cancer 2012; 106(5): 867–875